HIGH-FREQUENCY MURINE ULTRASOUND PROVIDES ENHANCED METRICS OF BAPN-INDUCED AAA GROWTH
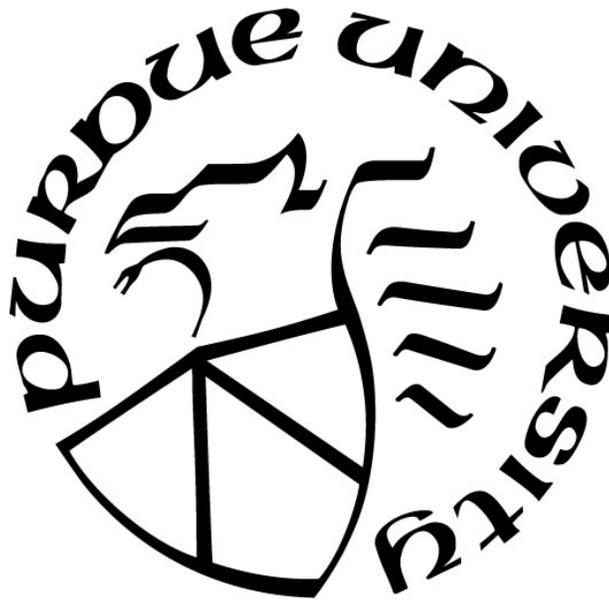
by

Daniel J. Romary

A Thesis

Submitted to the Faculty of Purdue University

In Partial Fulfillment of the Requirements for the degree of

Master of Science in Biomedical Engineering

Weldon School of Biomedical Engineering

West Lafayette, Indiana

May 2019

THE PURDUE UNIVERSITY GRADUATE SCHOOL
STATEMENT OF COMMITTEE APPROVAL

Dr. Craig J. Goergen, Co-Chair
> Weldon School of Biomedical Engineering

Dr. Sherry L. Voytik-Harbin, Co-Chair
> Weldon School of Biomedical Engineering

Dr. Charles F. Babbs
> Weldon School of Biomedical Engineering

Approved by:
> Dr. George R. Wodicka
>> Head of the Graduate Program

For the scientific advancement of medicine and the greater glory of God.

"If I have seen further than others, it is by standing upon the shoulders of giants."

– Sir Isaac Newton

ACKNOWLEDGMENTS

First, I especially want to thank my committee. Dr. Craig Goergen has been a fantastic PI who has provided me with the resources, independence, and confidence to succeed. Dr. Sherry Harbin was the first person to expose me to research, and she has taught me much about the scientific process. Dr. Charles Babbs is a tremendous teacher and pioneer in the field whom I have had the honor of getting to know.

I'd also like to thank Purdue University. The Charles C. Chappelle fellowship completely funded my Master's education, and my research would not have been possible without the facilities at Purdue. My experiences here have also allowed me to build relationships with inspirational trustees, administrators, faculty, staff, students, and alumni, for which I am ever grateful.

I also sincerely appreciate the other members of the Cardiovascular Imaging Research Laboratory, who have been invaluable resources in the brainstorming and troubleshooting that was necessary to complete this work.

Lastly, I want to thank my family, especially my parents. They are responsible for providing the foundation I needed in order to be successful. I do not take their continued support and encouragement for granted.

TABLE OF CONTENTS

LIST OF FIGURES

LIST OF ABBREVIATIONS

4DUS = Four-dimensional ultrasound

α-SMA = Alpha smooth muscle actin

AAA = Abdominal aortic aneurysm

B+E = BAPN + elastase group

B-mode = Brightness mode ultrasound

BAPN = β-aminopropionitrile fumarate salt

E = Elastase-only group

ECG = Electrocardiogram

EKV = ECG-gated kilohertz visualization

H&E = Hematoxylin & eosin

HI = Heat-inactivated elastase group

LOX = Lysyl oxidase

M-mode = Motion mode ultrasound

MPC = Movat's pentachrome

ROI = Region of interest

ABSTRACT

Author: Romary, Daniel, J. MSBME
Institution: Purdue University
Degree Received: May 2019
Title: High-Frequency Murine Ultrasound Provides Enhanced Metrics of BAPN-Induced AAA Growth
Committee Chair: Craig Goergen, PhD, & Sherry Voytik-Harbin, PhD

An abdominal aortic aneurysm (AAA), defined as a pathological expansion of the largest artery in the abdomen, is a relatively common disease that frequently leads to death if rupture occurs. Once diagnosed, clinicians often evaluate the rupture risk based on the maximum diameter of the aneurysm, a limited metric that is not accurate for all patients. In this study, we worked to provide additional distinguishing factors between growing and stable AAAs to aid in clinical rupture risk assessment. We utilized a relatively new murine model that uses surgical application of topical elastase to cause initial aortic expansion, and a lysyl oxidase inhibitor, β-aminopropionitrile (BAPN), in the drinking water to promote AAA growth. We further sought to develop and demonstrate applications of advanced imaging approaches, including four-dimensional ultrasound (4DUS), to obtain and evaluate alternative geometric and biomechanical parameters between 1) growing AAAs, 2) stable AAAs, and 3) non-aneurysmal control mice. Our study confirmed the reproducibility of the model and found reduced strain values, greater tortuosity, and decreased elastin health in mice with aneurysms. We also found expanding murine AAAs to have increased peak wall stress and surface area per length compared to stable aneurysms. The results from this work help provide a better understanding of the growth patterns associated with elastase-BAPN murine aneurysms and demonstrate the capabilities of high-frequency ultrasound. Eventually these data could help lay the groundwork for improving insight into clinical prediction of AAA expansion.

1. INTRODUCTION

1.1   Abdominal Aortic Aneurysms

An abdominal aortic aneurysm (AAA) is a pathologic condition characterized by a dilation of the abdominal aorta. This disease is relatively common, affecting approximately 1.4% of those between 50 and 84 years of age in the United States, or 1.1 million people [1]. AAAs are especially common among men and those with a history of smoking [1-3]. They often occur in the infrarenal aorta [4, 5], and are most commonly fusiform in shape [1]. Mechanistically, elastin is degraded within the medial layer [6], collagen content is altered [6-9], inflammatory cells infiltrate the tissue [10], and matrix metalloproteinase levels elevate [5]. AAAs are also associated with atherosclerotic plaques and intraluminal thrombus [5], but the causal relationship between aneurysms and other vascular disease is not completely understood.

While dilation itself is often externally asymptomatic, the major concern is aneurysm rupture, where massive internal hemorrhaging causes 90% of rupture patients to die before reaching the hospital [11]. When an AAA is detected prior to rupture, clinicians must decide whether to treat the AAA or watch and wait. Both options have their risks. The current treatment options are open surgical intervention or endovascular repair. Although the endovascular approach, in which a stent graft is deployed through a catheter, is associated with a lower procedure mortality rate than open repair, there is a significant risk of future complications due to endograft leaks and failures [12]. Alternatively, surveilling the AAA can also be risky, given the high mortality rate associated with rupture and the psychological harm a AAA diagnosis can cause [13].

Updated 2018 guidelines from the Society for Vascular Surgery regarding treatment indication attempt to incorporate many different risk factors, but the most widely adhered-to metric is maximum diameter. Maximum diameter is defined as "the maximum transverse dimension measured orthogonal to the vessel axis," as measured by ultrasound or computed tomography (CT) [1]. The guidelines state that an AAA should be repaired if its maximum diameter is greater than 5.4 cm, and conversely suggest that an AAA should be surveilled if its maximum diameter is less than 4.0 cm [1]. This metric is obviously not perfect because, aside from the ambiguous middle

range, many aneurysms rupture before reaching the upper threshold and many more would likely not rupture until well after that diameter [14]. Given the ambiguity regarding overall intervention criteria, finding more accurate metrics for rupture risk assessment is a clear unmet clinical need.

In order to identify these metrics, a better understanding of the mechanisms underlying AAA progression and rupture is required. Small animal models have become an important component of studying AAAs, because they allow for large scale, relatively inexpensive, controlled experiments to evaluate specific mechanisms. A wide variety of models exist, many emulating parts of AAA pathophysiology well, but none encompassing all human characteristics. These models include intraluminal perfusion of elastase [15, 16], topical application of calcium chloride [16, 17], and infusion of angiotensin II in genetically altered hyperlipidemic mice to create dissecting suprarenal AAAs [16, 18]. A relatively new model topically applies elastase to degrade medial elastin and uses a lysyl oxidase (LOX) inhibitor, β-aminopropionitrile (BAPN), in the drinking water to promote sustained AAA growth [19]. Here we investigate indicators of AAA expansion using this new model in order to ultimately help improve decision metrics beyond maximum diameter.

1.2   Ultrasound

Ultrasound is an important clinical tool in AAA detection and monitoring in both humans and small animals. In fact, according to the Society for Vascular Surgery, ultrasound is the preferred imaging modality for aneurysm screening and surveillance [1]. Ultrasound has achieved this status because it is noninvasive, widely available, and inexpensive [20]. Historically, it has allowed for consistent measurement of the aorta to identify and monitor AAA formation and progression. Recent developments in ultrasound imaging now allow for the advanced biomechanical and geometric image analysis that is demonstrated in this thesis.

Standard ultrasound images are typically brightness mode (B-mode), where the pixel brightness is proportional to the acoustic impedance of the tissue being imaged. This allows for two-dimensional viewing of anatomical structures either in long axis, parallel to the centerline of the structure, or in short axis, viewing a perpendicular cross section. Another common image type is motion mode (M-mode), which shows motion of one location over time. This technique is useful

for viewing arterial pulsation over the cardiac cycle. ECG-gated kilohertz visualization (EKV) is another methodology specific to VisualSonics ultrasound systems that is well suited for viewing structures over the cardiac cycle. In this technique, multiple images are collected across the cardiac cycle, then reconstructed to obtain an image with two spatial dimensions and one temporal.

Our laboratory has pioneered yet another technique that combines volumetric ultrasound and cardiac gating. Four-dimensional ultrasound (4DUS) collects 2D EKV images slice-by-slice over a prescribed distance, followed by reconstruction of the data to visualize three spatial dimensions over the cardiac cycle. This technique was developed and validated imaging murine hearts [21, 22], but can be applied to vasculature by taking long-axis images over the width of the vessel or short axis images over its length [23].

1.3 Geometric Indices Beyond Maximum Diameter

The acquisition of four-dimensional data (x,y,z,t) allows us to calculate more advanced metrics beyond simple diameter measurements. One such metric is tortuosity. Several studies have confirmed that tortuosity is increased in ruptured AAAs [24, 25], suggesting that complex flow patterns and vascular mechanics may place patients at increased risk. Further, increased AAA surface area has also been correlated with increased rupture [26]. Although surface area is likely a function of maximum diameter, it offers a more descriptive view indicating both the size of the AAA and the length of aorta that is aneurysmal. These and other geometric indices are not yet widely studied, but they are becoming of greater interest due to their implications on the biomechanics of the aorta.

1.4 Biomechanics

Advanced biomechanics is one of the leading areas of research for finding an alternative to the maximum diameter criterion. Because the main concern is rupture – a mechanical failure of the wall – it is logical that biomechanical quantities could serve as indicators of AAA growth and rupture. Two of the most common indicators are vessel wall strain and stress.

1.4.1 Strain

Cyclic strain is perhaps the most widely used and reported biomechanical index, likely due to its relative ease of estimation. Strain can be thought of as a measure of distensibility or deformation. Clinicians often use the linear definition of strain, where a change in length is divided by a reference length. In vascular medicine, the change in length corresponds to the change in radius or cross-sectional area over the cardiac cycle, and the reference length is often the diastolic radius or area. This definition is derived from a simplification of the Green-Lagrange strain tensor that is accurate only when strain magnitude is small [27]. The Green-Lagrange strain tensor (E) is shown in Equation 1, with the circumferential component ($E_{\theta\theta}$) for a cylinder shown in Equation 2, where F is the deformation gradient tensor, I is the identity matrix, and r is the radius at systole and diastole, respectively [28, 29].

$$E = \frac{1}{2}[F^T \cdot F - I] \tag{1}$$

$$E_{\theta\theta} = \frac{1}{2}[(\frac{r_{sys}}{r_{dia}})^2 - 1] \tag{2}$$

Because of the quadratic term, Equation 2 accurately describes large deformations, and is therefore the preferred method of calculating circumferential strain in the vessel wall in this thesis. In practice, strain can be calculated using M-mode ultrasound to obtain vessel parameters, such as diameter or radius, in systole and diastole [30]. Speckle tracking and direct deformation estimation are also emerging approaches to estimate the full three-dimensional strain tensor [31-33].

For both mice and humans, the peak circumferential cyclic strain in a healthy infrarenal aorta is on the order of 12-20% [30, 34]. Because elastin is degraded in AAAs, peak cyclic strain can be reduced to less than 5% in humans with AAAs [31], depending on the stage of the aneurysm. These drastic changes in strain make it a desirable trait to measure and understand over time, and a potentially important component of an accurate animal model.

1.4.2 Stress

Wall stress is another biomechanical metric caused by intraluminal pressure and residual stress within the vessel wall [35]. The circumferential component, also called hoop stress, is of interest because by definition, the aorta will rupture when this wall stress exceeds the strength of the wall [36].

Circumferential stress can be calculated according to the Law of Laplace, which is shown in Equation 3 [37]:

$$Stress = \frac{Pressure * Radius}{Wall\,Thickness} \tag{3}$$

This equation assumes a perfect thin-walled cylinder where the stress distribution is uniform throughout. Although this may be an oversimplification, this calculation has been performed in multiple human studies and is a common clinical approach [38, 39]. Although a significant challenge for any stress calculation is obtaining accurate wall thickness *in vivo* [40], the three basic parameters in the Laplace equation can often be estimated or obtained *ex vivo* depending on the study. Further, this law serves as the foundation for the maximum diameter criterion used to determine when surgery is warranted [41]: if pressure and thickness are assumed to be constant, then peak stress is a function of only the maximum radius. The problem is that pressure and thickness may not always be constant; hence, evaluating stress may be more representative and beneficial than maximum diameter alone.

More recent analyses typically use Finite Element Analysis (FEA) to calculate wall stress at many points along the aorta by solving complex governing differential equations [42]. As one could expect, this technique requires more information and computational power than the Law of Laplace. It also often requires additional assumptions to be made and robust constitutive models to be adopted, which can greatly affect the accuracy of the calculation [43]. Regardless of the equations used, multiple studies in humans have found increased wall stress to be indicative of rupture [11, 38, 44]. Additional research is also being undertaken to understand the role of stress in AAA expansion [45, 46] and extracellular matrix changes [47]. This popular area of research is therefore an important one, in need of advances in methodology and understanding.

2. BAPN-INDUCED AAA GROWTH STUDY

2.1 Introduction

There is a clear clinical need for more robust and accurate risk indicators for AAA rupture beyond basic diameter measurements [36, 41, 48]. Assuming a rapidly growing AAA is one that will eventually rupture, the driving motivation of this study is to identify differences between growing and stable AAAs toward alternative criteria for rupture risk assessment.

Specifically, a relatively new murine model will be used to create these growing and stable aneurysms. The BAPN-elastase model, first published in 2017 [19], uses topical elastase to create an AAA and adds BAPN to the drinking water to promote AAA growth. Elastase breaks down medial elastin and causes an inflammatory response [49], leading to the formation of a stable AAA when applied by itself [19, 49]. But when BAPN, a LOX inhibitor that prevents crosslink formation within and between elastin and collagen [50], is also incorporated, a chronic, growing AAA is created [19]. However, BAPN alone, without active elastase, has been found to have no effect on the size of the aorta at the stated concentration [19]. Therefore, BAPN combined with heat-inactivated elastase can be evaluated as a negative control, accounting for generic surgical effects and providing insight into the impact of LOX inhibition. Moreover, by using this study design to evaluate stable AAAs, growing AAAs, and control aortae in a longitudinal study, we can also achieve a secondary goal of further characterizing a relatively new mouse model of AAAs [19].

By using this mouse model, we can also further develop and demonstrate newer techniques in ultrasound imaging and data analysis. An entire ultrasound workup will be completed at each time point, including 4DUS. These novel techniques will allow us to estimate advanced geometric indices, such as tortuosity and surface area, and biomechanical metrics, such as strain and stress. By identifying the relationships between these indices and AAA growth, we can potentially move rupture risk assessment beyond maximum diameter. Furthermore, these estimations will advance the basic science field because the initial work on this murine model only described metrics such as diameter and inflammation [19].

Overall, while the results from this study will eventually need to be compared to clinical data, the investigation described here will improve our understanding of aneurysm disease through the use of a newly created animal model, imaging and analysis methods capable of producing enhanced metrics, and greater insight into why some AAAs grow while others remain stable.

2.2 Materials and Methods

2.2.1 Experimental Design Overview

Ten-week-old male C57BL/6J mice (Jackson Laboratories, Bar Harbor, ME) were divided into three experimental groups to investigate stable aneurysms, growing aneurysms, and a control of healthy size. Specifically, the elastase group (E; $n=6$) underwent surgery to apply topical elastase and create a stable aneurysm [49, 51]. The BAPN-elastase group (B+E; $n=5$) underwent topical elastase surgery and also received 0.2% β-aminopropionitrile fumarate salt (BAPN) in their drinking water throughout the study, beginning two days prior to surgery [19]. As a negative control, a heat-inactivated (HI) group ($n=5$) also underwent surgery and received BAPN in the drinking water, but the topical elastase applied was inactivated by heating to 100°C for 30 minutes prior to use [19]. All animals were tracked for four weeks after surgery (Figure 1).

2.2.2 Surgical Procedure

All animal procedures were approved by the Purdue Animal Care and Use Committee. Animals were anesthetized with 1-3% isoflurane in 1 L/min medical grade air and underwent an open laparotomy. After retracting the other organs, approximately 4 mm of the infrarenal aorta was exposed from the surrounding supportive tissue through blunt dissection with forceps. 5 μL of porcine elastase (E7885, Sigma Aldrich, St. Louis, MO) at a concentration of 5 mg/mL was applied via a micropipette and allowed to remain for five minutes before flushing with 1 mL saline three times. The abdomen was closed with sutures in the muscle and skin layers, and the animals recovered without complication.

2.2.3 Weekly Monitoring

We conducted ultrasound imaging every week after surgery for four weeks, and at baseline before surgery. A Vevo 2100 system (FUJIFILM VisualSonics Inc., Toronto, ON, Canada) with a 32-55

MHz frequency transducer (MS550D, 40 MHz center frequency) was used for ultrasound imaging. We performed a full ultrasound workup each week, which included standard B-mode and EKV images in long axis, along with M-mode images in the middle of the aneurysm. 4DUS was also acquired in short axis, collecting serial EKV images from the left renal vein to the aortic bifurcation.

Time domain records of blood pressure were also collected at baseline and at 2, 3, and 4 weeks to establish systolic and diastolic levels using a tail cuff measurement system (CODA-HT2, Kent Scientific, Torrington, CT). We followed manufacturer instructions similar to published protocols [52], placing the animal on a heated stage without anesthesia within a restraint. After occluding the tail and gradually deflating, the system uses a volume pressure recording sensor to identify the pressure with the minimum rate of change of blood volume as systole, and the pressure with the maximum rate of change of blood volume as diastole [52]. At least 20 measurements where these two points were correctly identified after an acclimation period were averaged for estimates of systolic and diastolic blood pressure, respectively.

2.2.4   Histology and Immunohistochemistry

After euthanasia via isoflurane overdose and bilateral pneumothorax, the aorta and kidneys were harvested from each animal and fixed. Serial cuts were made every 2-3 mm along the infrarenal aorta in order to embed the resulting tissue in paraffin. Sections of 4 micrometers were stained with hematoxylin and eosin (H&E) and Movat's pentachrome (MPC). In the MPC images, elastin is stained black, collagen is yellow, and muscle is red. To better discern the composition of the purple layer seen in the MPC images, additional slides were also stained for alpha smooth muscle actin (α-SMA), with smooth muscle showing as reddish brown, with a light blue counterstain.

We quantified the MPC histology in two ways. First, the medial layer (purple) and adventitial layer (yellow) were outlined in ImageJ (NIH, Bethesda, MD) to obtain average thickness measurements by using the perimeter as a circumference and assuming the vessel was circular. Secondly, to better evaluate characteristic changes in the aortic walls of these groups, we employed a semi-quantitative scoring methodology. Specifically, one image within each quadrant of the aorta was taken at 40x magnification. Four individuals scored the images in a blinded and randomized fashion on a scale of 1 to 5, where 5 corresponded to healthy elastin sheets present, 3 corresponded

to degraded or unhealthy elastin fragments present, and 1 corresponded to no elastin present. All four individuals' scores were averaged together for each image.

2.2.5 Ultrasound Image Analysis

At every time point we calculated the maximum cross-sectional area of the aortic lumen, from which the diameter was estimated as a maximum effective diameter assuming a perfect circle (VevoLab, FUJIFILM VisualSonics Inc.). Using M-mode ultrasound, three randomly selected cardiac cycles were measured to find the average systolic and diastolic diameters near the middle of the aneurysm. These measurements from M-mode were used to calculate the Green-Lagrange circumferential cyclic strain according to Equation 2 (section 1.4.1).

Serial EKV images were reconstructed and interpolated using MATLAB to produce a 4D dataset with isotropic voxels. This dataset was loaded into SimVascular, where the lumen at systole and diastole were manually segmented to create 3D models of each [53]. These 3D models were loaded back into MATLAB to calculate tortuosity, surface area, and strain. Specifically, at every z-slice of the models, equal to 0.05 mm, the area of the lumen at diastole and systole were extracted and converted to radii for use in the Green-Lagrange circumferential cyclic strain equation.

2.2.6 Statistical Analysis

Data are shown as mean ± SD and statistical analysis was performed in Prism (v7.0d, GraphPad, San Diego, CA). Unless otherwise noted, a two-way repeated-measures analysis of variance (ANOVA) with post-hoc Tukey tests was performed with an overall type I error rate of $\alpha=0.05$. Following standard conventions, all graphs use $*p \leq 0.05$, $**p \leq 0.01$, $***p \leq 0.001$, and $****p \leq 0.0001$.

2.3 Results

2.3.1 Diameter Measurements Justify Experimental Group Design

To evaluate the successful creation of our experimental groups based on size, we calculated the maximum effective diameter at every time point (Figure 2A). Qualitatively, the HI mice aortae remained approximately the same size, E mice aortae dilated but plateaued at 198 ± 38% of their

original size, and B+E mice aortae were on an upward trajectory, expanding to $364 \pm 93\%$ of their original size at the study end point.

The AAA growth rates (Figure 2B) revealed that the E and B+E groups expanded rapidly in the first week. Then starting at Day 14, the growth rate of E mice was not significantly different than that of the HI group, indicating that the E group was stable. The B+E mouse growth rate was significantly greater than the HI rate for all time points. Overall, the HI group can be considered a negative control with aortae at a healthy size, the E group can be considered a stable aneurysm starting at Day 14, and the B+E group can be used to assess continually expanding AAAs. Because the E group takes up to 14 days to stabilize, we focused our analysis on Days 14, 21, and 28. Longitudinal long axis ultrasound images of a representative animal in each group can be found in the appendix (Figure S1).

2.3.2 Strain Reduction After Elastase Application

To assess differences in distensibility between the groups, M-mode ultrasound was used. Qualitatively, aneurysmal vessels appeared to distend less than vessels in control mice (Figure 2C) and quantitatively, circumferential strain decreased significantly for both E and B+E groups ($p <$ 0.001; Figure 2D). All three groups have similar baseline strain values of roughly 11%. Once elastase has been applied, regardless of whether the aneurysm is growing, there is a reduction in mean strain to about 2.5%, while the HI group remains near baseline.

Taking advantage of our 4DUS data, we calculated strain every 0.05 mm along the aorta (Figures 3A, S2, and S3). From these maps, the strain appears heterogenous, but with overall lower strain values in aneurysmal regions and higher values in healthy regions. In order to quantitatively compare between experimental groups, we estimated strain within a region of interest (ROI). For animals with AAAs, a band 1 mm in height was placed at the maximum diameter, excluding regions of great tortuosity or rapid expansion/contraction. Strain values within this band were then averaged per animal for comparison. For the baseline images and the HI group at all time points, a band 4 mm in height halfway between the iliac bifurcation and the renal vein was used as the ROI as an estimate of where elastase was applied surgically. The averaged strain values (Figure

3B) appear markedly similar to the values from M-mode (Figure 2D). Significant reductions in strain were noted in both groups where elastase was applied.

To fully describe the distribution of strain values along the entire infrarenal aorta, we generated a cumulative frequency plot for all animals at Day 28 (Figure 3C). By fitting a sigmoidal curve and estimating the inflection point, corresponding to the median strain value for each group, all three groups are significantly different from one another ($p < 0.0001$). The HI group has the largest median (8%), followed by the E group (4%), then the B+E group shifted the farthest left (0%).

2.3.3   3D Models Provide Geometric Data

Another advantage of creating three dimensional models of the aorta is the ability to obtain geometric information. To evaluate tortuosity, the centerline of each aorta at diastole on Day 28 is displayed and separated by group (Figure 4A). The centerlines appear more variable and tortuous for the two AAA groups. Tortuosity was quantified as the centerline length divided by the Cartesian distance between the highest and lowest point (Figure 4B). A perfectly straight vessel has a tortuosity of 1. While the HI group is not perfectly straight, the AAA groups are significantly more tortuous at Day 14, Day 21, and Day 28 ($p < 0.05$). Although the E and B+E groups are not significantly different from one another, it appears that B+E mice could be trending towards significantly higher tortuosity at later timepoints.

To compare an additional geometric index, a surface area per length metric was calculated by dividing the diastolic lumen surface area by the centerline length. The B+E group had significantly greater surface area per length than the HI control at all aneurysmal time points (Figure 4C, $p < 0.01$). It was also significantly greater than the stable aneurysm group at Days 21 and 28 ($p < 0.01$). Although the average surface area per length of the E group was greater than the average of the control at all aneurysmal time points, it was only significant at Day 21 ($p < 0.05$).

2.3.4   Histology Reveals Changes in Aortic Wall Composition After AAA Formation

To understand the microscopic impacts of the treatments, we performed a histopathological analysis (Figure 5A). The HI samples stained with MPC reveal healthy, black elastin organized in four lamellar units. The α-SMA staining confirms that much of the purple medial layer is

comprised of smooth muscle cells. There is also a yellow band of adventitial collagen surrounding this medial layer in all slides.

In some mice in the E group the medial layer seems to almost disappear, showing little smooth muscle cell or elastin. In other mice in both the E and B+E groups, the medial layer is present, but the elastin does not have its quintessential healthy waviness. Instead elastin fibers appear small, linear, and scattered throughout the media.

The semi-quantitative scores from all four quadrants were averaged together to compare representative elastin health for each animal (Figure 5B, left). Alternatively, to further evaluate the worst level of degradation, each animal's minimum quadrant score is also graphed (Figure 5B, right). These data reveal significantly lower elastin scores for the groups with AAAs, both average and minimum scores ($p < 0.001$). E and B+E average quadrant scores have similar group-wise means of 2.7 ± 0.3 and 2.8 ± 0.5 out of 5, respectively. For minimum quadrant scores, although the difference is not significant, the E group has a mean of 1.7 ± 0.7, whereas the B+E group mean is 2.0 ± 0.4.

From the average thickness measurement, we found that the average transmural thickness increases with the size of the aorta (Figure 5C). The medial thickness increases for the B+E group compared to the control ($p < 0.05$), and increased levels of collagen are also present in the adventitia of both AAA groups ($p < 0.001$).

2.3.5 Wall Stress Estimation Reveals Increased Stress in Growing AAAs

Figure 6A displays the systolic blood pressure (SBP) for each animal at all time points. Each animal's SBP was averaged over the four time points, to obtain one value per animal for stress calculations (Figure 6B).

In addition, we first used the maximum effective radius from ultrasound images at Day 28, and the average transmural thickness from a representative MPC image for the animal to obtain an estimate of maximum circumferential wall stress (Figure 6C). The B+E group had higher transmural stress compared to mice in the HI group ($p < 0.05$). Using the thickness of only the adventitia instead of

the whole wall, significantly higher stress was found in the B+E group compared to the E group ($p < 0.05$, Figure 6D).

2.4 Discussion

Here we sought to evaluate differences between growing and stable AAAs in a relatively new murine model using advanced ultrasound techniques. This model repeatably produces AAAs in the infrarenal aorta, the site most commonly associated with AAAs in humans. In accordance with previously published results [19], BAPN by itself at a concentration of 0.2% has negligible effects on the vasculature. Specifically, in relation to diameter, the HI group remained at a constant, non-aneurysmal size throughout our study. We also confirmed that biomechanical and geometric characteristics were not affected by BAPN alone, as the HI group did not change from baseline. Histological images of the HI group also appeared within normal limits, indicating that LOX inhibition by itself at 0.2% does not have an effect on wall structure. Therefore, the HI group can indeed be considered a healthy negative control for the purposes of this study.

In terms of diameter, the two other experimental groups also reproduced the effects of elastase [19, 51] and the combination of BAPN and elastase [19]. Specifically, initial expansion seems to be dependent on elastase application, but ongoing AAA growth appears to be correlated with LOX inhibition.

Previously-published literature has shown a reduction in strain in elastase-induced aneurysms as measured by M-mode [54, 55] and biomechanical specimen testing [56]. Our results agree with these findings. Additionally, the growing aneurysms we created had similarly-reduced strain to the stable aneurysms ($p > 0.05$), with means less than 5%. This finding suggests that strain, although interesting, may not be a distinguishing factor between expanding and stable AAAs.

However, multiple studies have proven strain to be heterogeneous in AAAs, both in humans [32], and mice [23]. Therefore, it is desirable to obtain strain information at many locations along the aorta, as opposed to only one point, as in M-mode. We demonstrated this capability in the strain we measured from 4DUS (Figure 3). The results from this 4DUS strain calculation likewise reveal noticeable heterogeneity in strain throughout the aorta, both for healthy and aneurysmal aortas.

However, some areas around the shoulder regions, tortuous areas, and places with negative strain values are likely inaccurate due to segmentation artifacts or out-of-plane motion. Because of these inaccuracies, a ROI method helped improve the comparison between the three groups. The ROI averaged data compare well to the M-mode values, indicating reduced strain in aneurysmal regions and providing us with confidence in the results. In sum, this 4DUS strain calculation technique is a simple, computationally inexpensive method to obtain large amounts of strain data. Future methodologies could use a direct deformation estimation approach [33] to overcome some of the segmentation limitations, but this approach would require higher resolution imaging and greater computational power.

The other biomechanical metric evaluated in this study, peak circumferential wall stress, did correlate with AAA growth. Although we used the Law of Laplace, which makes substantial assumptions, it is a clinically relevant way of thinking that allows for a quick estimation of hoop stress based on the available parameters [57]. We also made efforts to ensure the accuracy of the parameters. Although our tail cuff estimation of blood pressure has been validated previously [58], these noninvasive measurements in mice are inherently noisy. In order to reduce the effects of the noise, and because there did not appear any significant longitudinal trends in the blood pressure, we used a longitudinal average for each animal. In addition, the histological results in Figures 5A and 5B suggest that the E and B+E groups did not possess functional elastin. Therefore, one can reasonably assume that the collagen of the adventitia was the component of the aortic wall that was experiencing nearly all of the stress. Following this logic, the Laplacian assumption of a single-layer, thin-walled cylinder is reasonably valid, and the data suggest increased stress in growing AAAs (Figure 6D).

Our wall stress findings align with published work in humans using both the Law of Laplace [38] and FEA [11, 44], suggesting that this parameter may be predictive of AAA rupture. Our study further confirmed that there are differences in aortic wall composition and thickness between stable and growing aneurysms; consequently, peak hoop stress may indeed be a better metric than diameter alone. Furthermore, as imaging techniques continue to improve, the wall thickness should be able to be measured via noninvasive approaches, making this metric more clinically relevant.

Aside from biomechanics information, our 4DUS imaging technique and creation of 3D models allowed for analysis of geometric indices of each aorta. Recently, work was published on a decision tree algorithm using geometric indices as inputs and AAA rupture as the output [26]. The findings suggested that various tortuosity metrics and surface area are significant indicators of AAA rupture [26]. Our study did not find differences in tortuosity between growing and stable AAAs, but it did find significant differences in the surface area per length metric. We divided the surface area by centerline length in order to control for differences in the length of the aorta due to animal differences or segmentation imprecision. Although surface area is in many ways a function of maximum diameter, it is a more descriptive approach that our data suggest is useful when volumetric imaging approaches are utilized.

One of the reasons for use of the elastase model is that elastin is degraded in human AAAs [6]. Previous studies found a correlation between aortic diameter, decreased elastin, and increased collagen content [9], in addition to the loss of a recognizable intimal layer intimal layer [41], which are similar to the results we report here. The first paper describing the elastase-BAPN model described elastin fragmentation, loss of smooth muscle cell order, and large amounts of collagen deposition in the elastase only group, with exaggerated findings in the BAPN + elastase group [19]. While we observed many of the same factors and did not observe much of a difference between E and B+E groups, there were some notable discrepancies from the previously published work. Specifically, the smooth muscle cells seemed to retain their layered order even without the elastin in both groups, and thick medial layers full of smooth muscle cells were especially observed in the B+E group. This thicker medial layer could be expected, as crosslinking is inhibited with BAPN. In addition, some regions of the aorta in the E group appeared to have no discernable media layers. In both groups where there was medial presence, elastin was obviously not functional; however, it is not clear whether the elastin seen in the histology is old, degraded elastin, or new, immature, *de novo* elastin that is not functional, suggesting the need for further examination.

In humans, LOX is downregulated in a condition called *cutis laxa* [50]. Elastin has been evaluated in the aortas of patients with this condition, and described as "irregular and stretched" in non-aneurysmal patients, and fragmented in those with AAAs [59]. One would expect the B+E group to have similar pathology, and although not an exact match, our results fit this description.

Therefore, the theory that the elastin seen in the B+E images is new elastin laid down could be justified as it has a stretched and fragmented appearance. However, additional analysis is needed to quantify the origin of the elastin and truly understand the implications of both treatment groups on the extracellular matrix.

The present study does have some limitations. Although this study did not seek to understand the role of intraluminal thrombus or atherosclerosis, this is a predominant feature of many AAAs [5] that was not present in most of the aneurysms we observed. However, our lab has completed preliminary studies that suggest increasing the concentration of elastase promotes thrombus formation. Therefore, this model could potentially be used to evaluate such lesions in future studies. The B+E model also does not produce AAA rupture within the study timeline, but it is a good choice for understanding AAA expansion, which itself is correlated with rupture [14, 60]. Additionally, our 4DUS strain methodology also has limitations. Specifically, we assumed that strain is uniform around the circumference, that the aorta is moving only in the radial direction during the cardiac cycle, and that the aorta centerline is orthogonal to the ultrasound beam. Although these claims are not always accurate, all three assumptions are also true of M-mode analysis, an approach that has been used clinically [30, 61]. Altogether, while there are limitations to the study, value can still be extracted from these findings.

In summary, strain decreased in aneurysmal aortas, tortuosity increased, and elastin health declined. Furthermore, growing AAAs had increased surface area per length and peak wall stress compared to their stable counterparts. These findings support the use of a relatively new murine model of AAAs, demonstrate the value of high frequency ultrasound capabilities, and contribute understanding of growing and stable AAAs to the medical community.

2.5 Figures
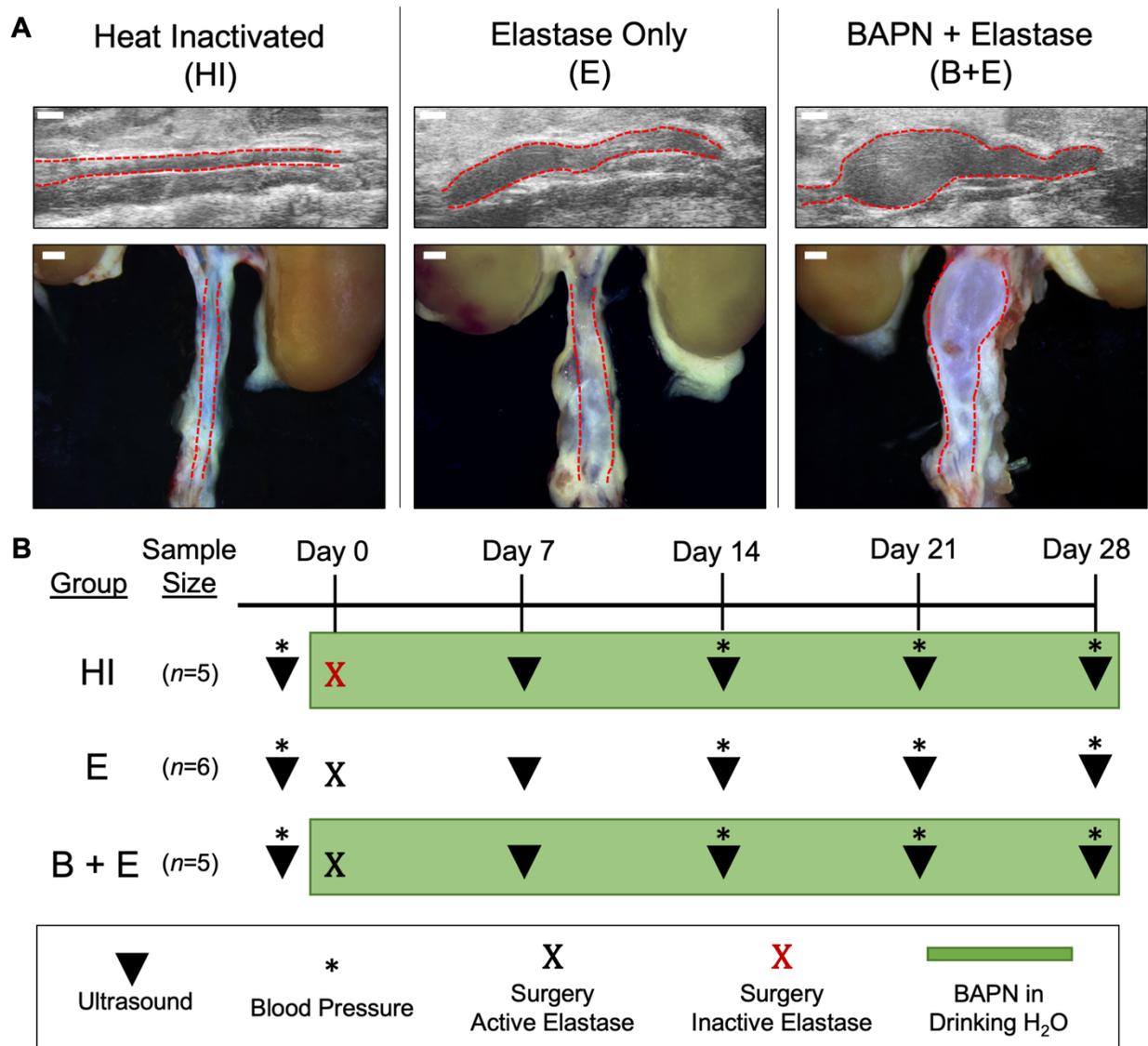
Figure 1. Experimental Groups. A) Day 28 ultrasound and gross anatomy images demonstrating HI as aorta of healthy size, E as stable aneurysm, and B+E as growing aneurysm. Dashed lines indicate aorta boundary. Scale bar = 1 mm. B) Timing schematic showing weekly imaging (triangle), blood pressure collection (*), and experimental differences between groups. Schematic also denotes surgery with 5 mg/mL active elastase (black 'x') and heat-inactivated elastase (red 'x'), and ongoing BAPN placed in drinking water (green box), with normal drinking water for the E group.
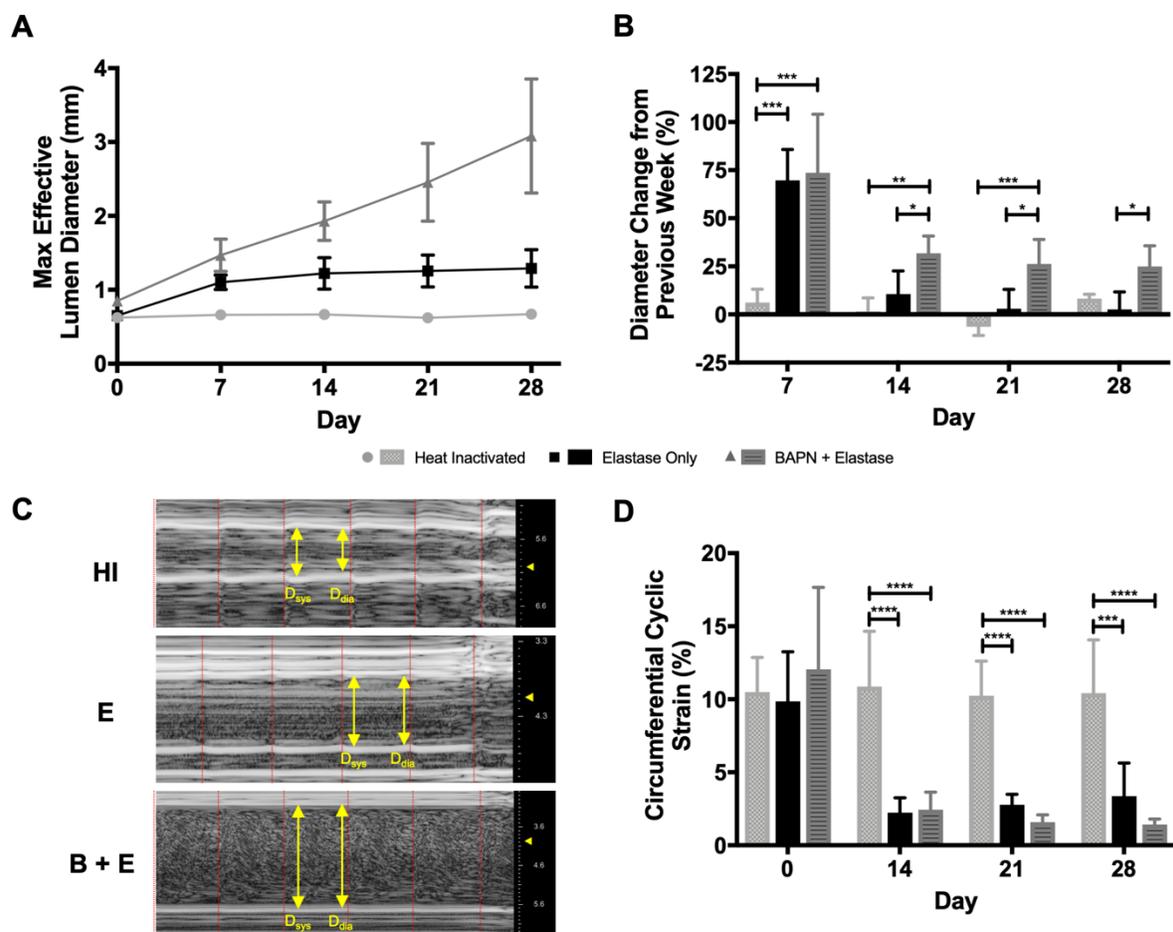
Figure 2. Simple Ultrasound Quantification. A) Maximum effective diameter of aortic lumen calculated from short axis ultrasound each week demonstrates three distinct experimental groups based on aortic size. Heat-inactivated group (SD smaller than marker size) remains a healthy size, whereas elastase with or without BAPN is enlarged. B) Percent change in lumen diameter from previous week demonstrates that, beginning at Day 14, BAPN caused significantly more growth than elastase only ($p < 0.05$), and elastase only is never significantly different from the heat inactivated control. C) Day 21 representative M-mode ultrasound images (units in mm), with arrows designating example systolic and diastolic points, and dashed lines bounding cardiac cycles. D) Green-Lagrange circumferential cyclic strain calculated from M-mode measurements reveals reduction of strain with elastase application ($p < 0.001$).
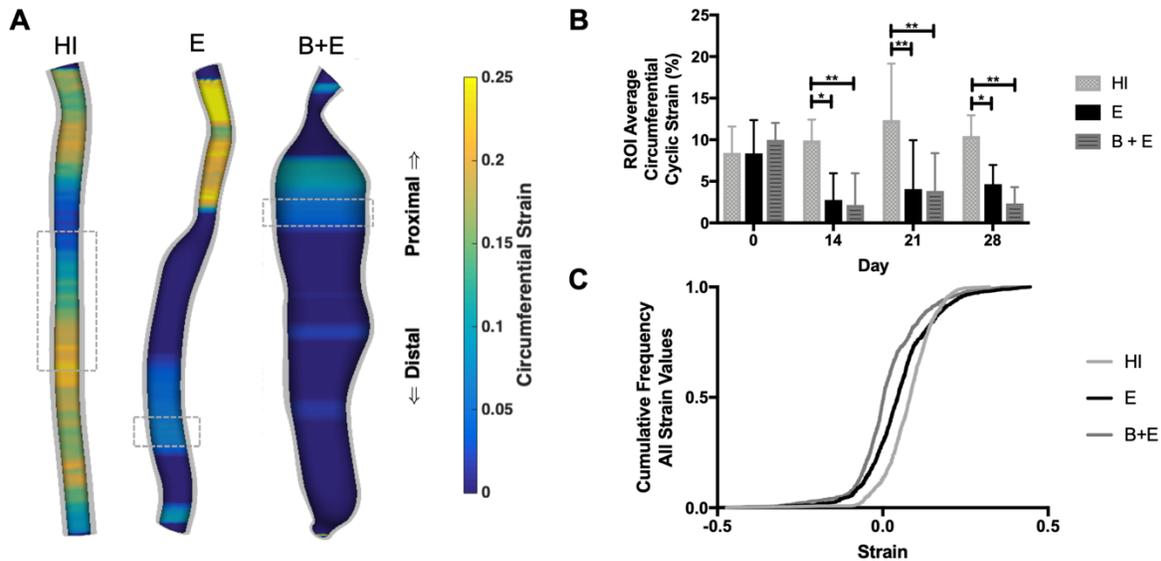
Figure 3. Advanced Ultrasound Quantification of Cyclic Strain Calculated at Each Z-slice of the Segmented Aorta Model. A) Visualization of strain at systole for representative animals at Day 28. Values outside of the color bar bounds are represented as the respective minimum or maximum. Boxes represent areas averaged for group-wise comparison in B. 4 mm height for HI, 1 mm for E and B+E. B) Average strain values from ROI in each animal reveal strain trends down once elastase is applied ($p < 0.05$), but no difference can be detected between growing and stable aneurysms. C) Distribution of all strain values along infrarenal aorta for all animals at Day 28 in the form of a cumulative frequency plot. Using inflection point from a sigmoidal fit, HI is shifted toward higher strain than E, which is higher than B+E ($p < 0.05$).
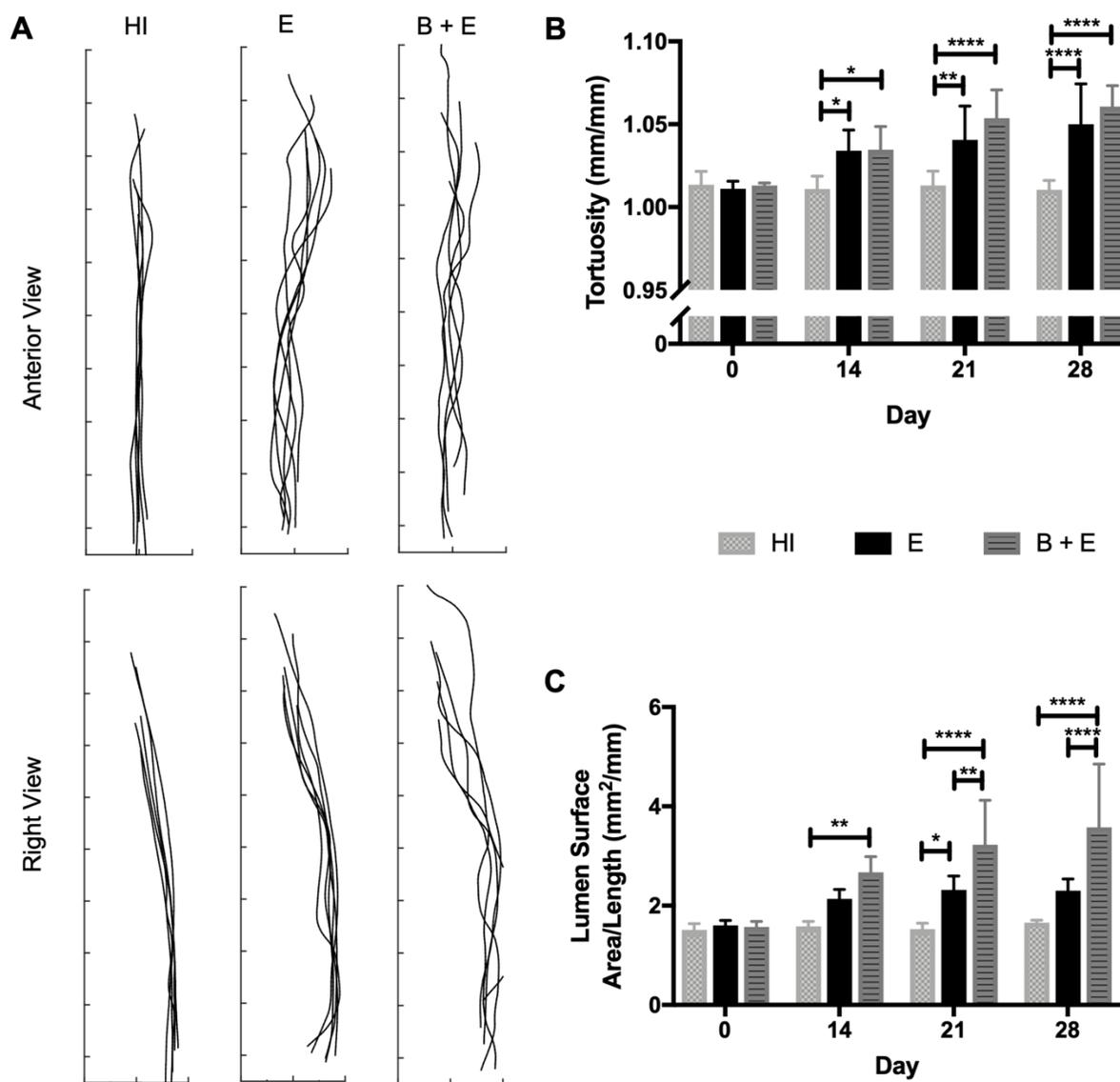
Figure 4. Advanced Ultrasound Quantification of Geometric Indices. A) Qualitative depiction of aorta centerlines at Day 28. Interval spacing 2 mm. B) Quantitative measure of diastolic aorta tortuosity (centerline length / height) over time, showing groups with AAAs are more tortuous. C) Longitudinal measurements of surface area of diastolic aortic lumen divided by centerline length, showing B+E group always had increased surface area/length once aneurysmal ($p < 0.01$).
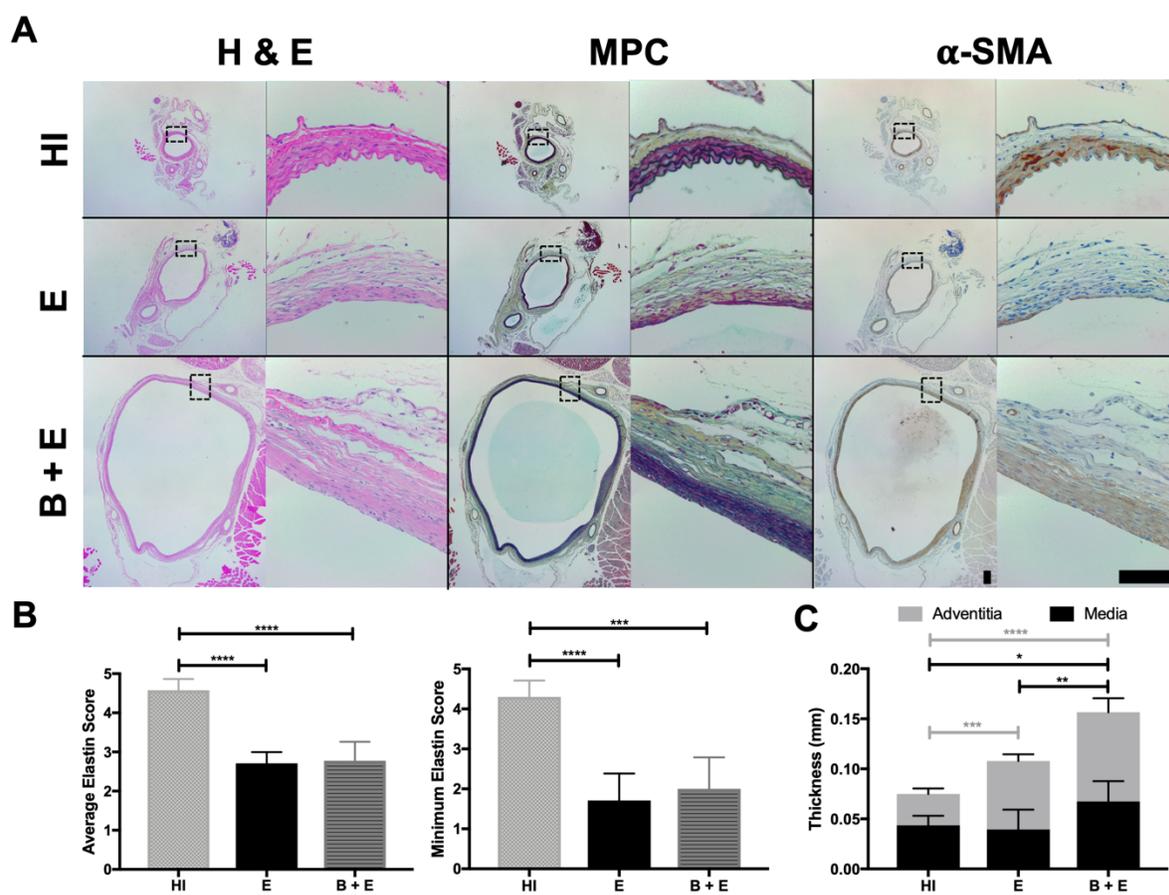
Figure 5. Histology and IHC. A) Hemotoxin & Eosin (H&E), Movat's Pentachrome (MPC), and alpha-smooth muscle actin (α-SMA) staining at 10x (left) and 40x (right) magnifications for heat-inactivated (HI), elastase only (E), and BAPN + Elastase (B+E) groups. 10x and 40x scale bars = 0.1 mm for all images. B) Results of semi-quantitative scoring analysis, where 5 = healthy elastin sheets present, 3 = degraded elastin fragments present, and 1 = elastin not present. Averaging all four quadrants (left) and using the minimum quadrant score (right) both reveal decreased elastin content in E and B+E groups. C) Aortic wall thickness from histology, as defined by medial and adventitial layers.
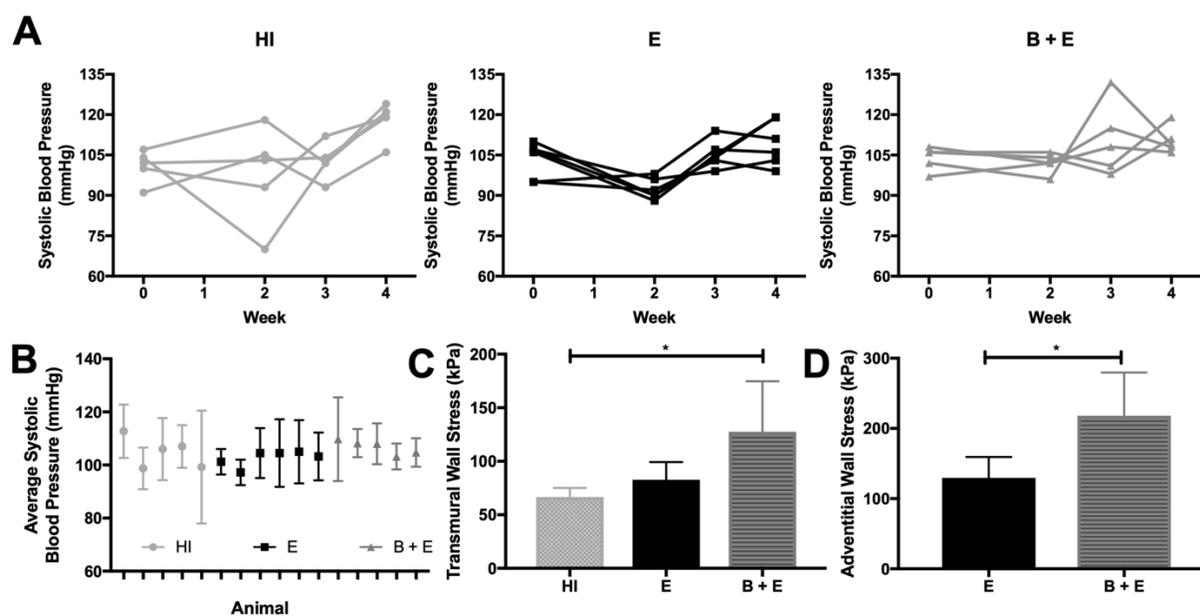
Figure 6. Peak Hoop Stress. A) Systolic blood pressure over time for each group. B) Systolic blood pressure averaged over time for each animal. C&D) Peak hoop stress calculated with pressure from B, maximum effective radius from ultrasound, and transmural (C) or adventitial (D) thickness from histology. If adventitia is assumed to carry most of the load due to elastin degradation, B + E has significantly greater hoop stress than E ($p < 0.05$).

3. CONCLUSIONS AND FUTURE DIRECTIONS

The motivation of this work was to better understand the differences between growing and stable AAAs to enhance rupture risk assessment. To that end, we found hoop stress and surface area per length to be significantly elevated in growing AAAs compared to stable ones, suggesting further evaluation of these specific parameters in humans. This work also provided significant insight into the recently developed BAPN-elastase model and demonstrated the value of advanced ultrasound techniques. Taken together, the results demonstrate a reduction in circumferential strain with elastase application, both from traditional M-mode and a novel 4DUS strain methodology. In addition, AAAs created with this animal model become tortuous and cause structural changes in the aortic wall, including decreased elastin health and increased adventitial thickness.

In order to translate this work into the clinic, future advances will be necessary. Namely, better strain estimation techniques without the need for substantial assumptions, in addition to accurate automatic segmentation tools, could provide more precision and accuracy in mapping aortic strain and detecting small differences between growing and stable AAAs. Advances in constitutive models, computational power, and machine learning techniques for finite element analysis [62], coupled with improved noninvasive ways to measure wall thickness [40] would also provide translatable ways to incorporate wall stress measurements into clinical decision making. Equipping clinicians with 4DUS systems has begun [63], but will need to become more widespread, with additional visualization and segmentation tools, in order to take advantage of its capabilities.

In the interim, the techniques demonstrated in this thesis could be applied to larger animals, and further corroborated with human data. Additional study is needed at the microscopic level to better characterize the extracellular matrix changes of this model. While much work will need to be done in the future to provide clinical risk assessment alternatives to maximum AAA diameter, this research should help improve our understanding of the effects of BAPN, exhibit the use of 4DUS in elastase induced AAAs, and demonstrate the utility of stress and strain quantification in experimental aneurysms.

APPENDIX

SUPPLEMENTAL FIGURES
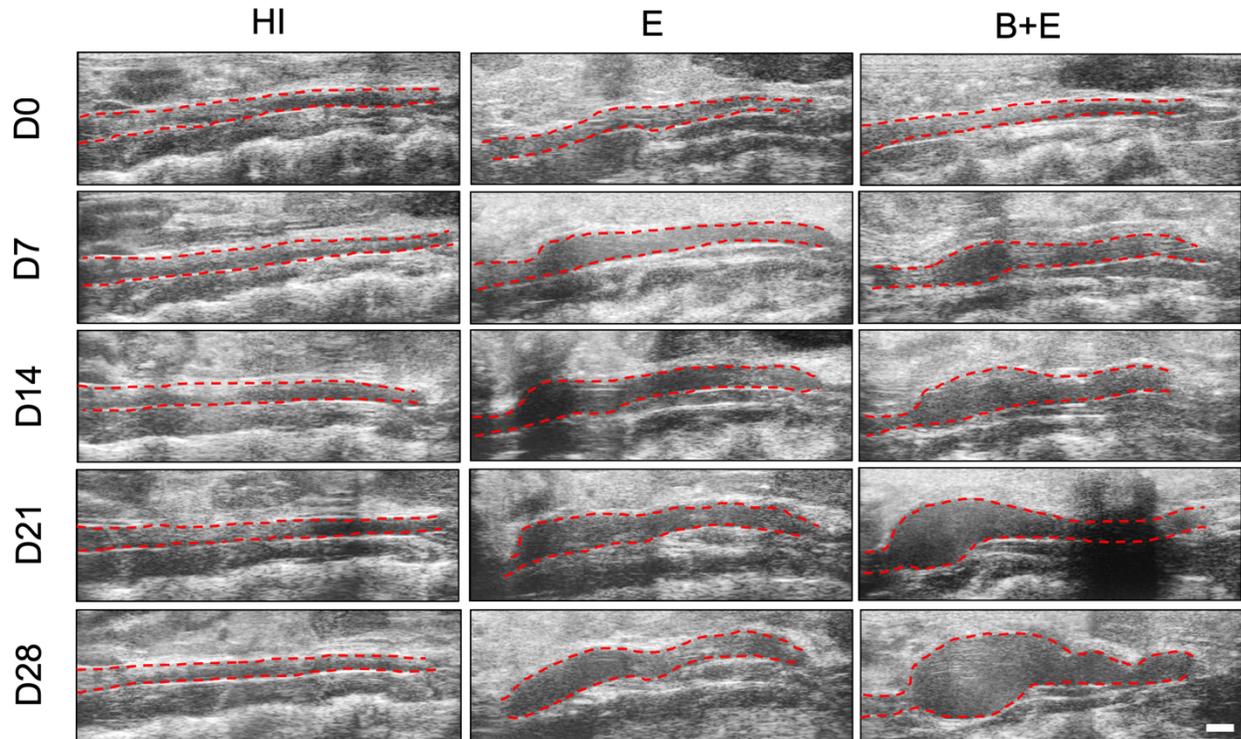
Figure S1. Longitudinal Ultrasound Imaging. Representative weekly ultrasound images for one animal in each experimental group. Scale bar = 1 mm.
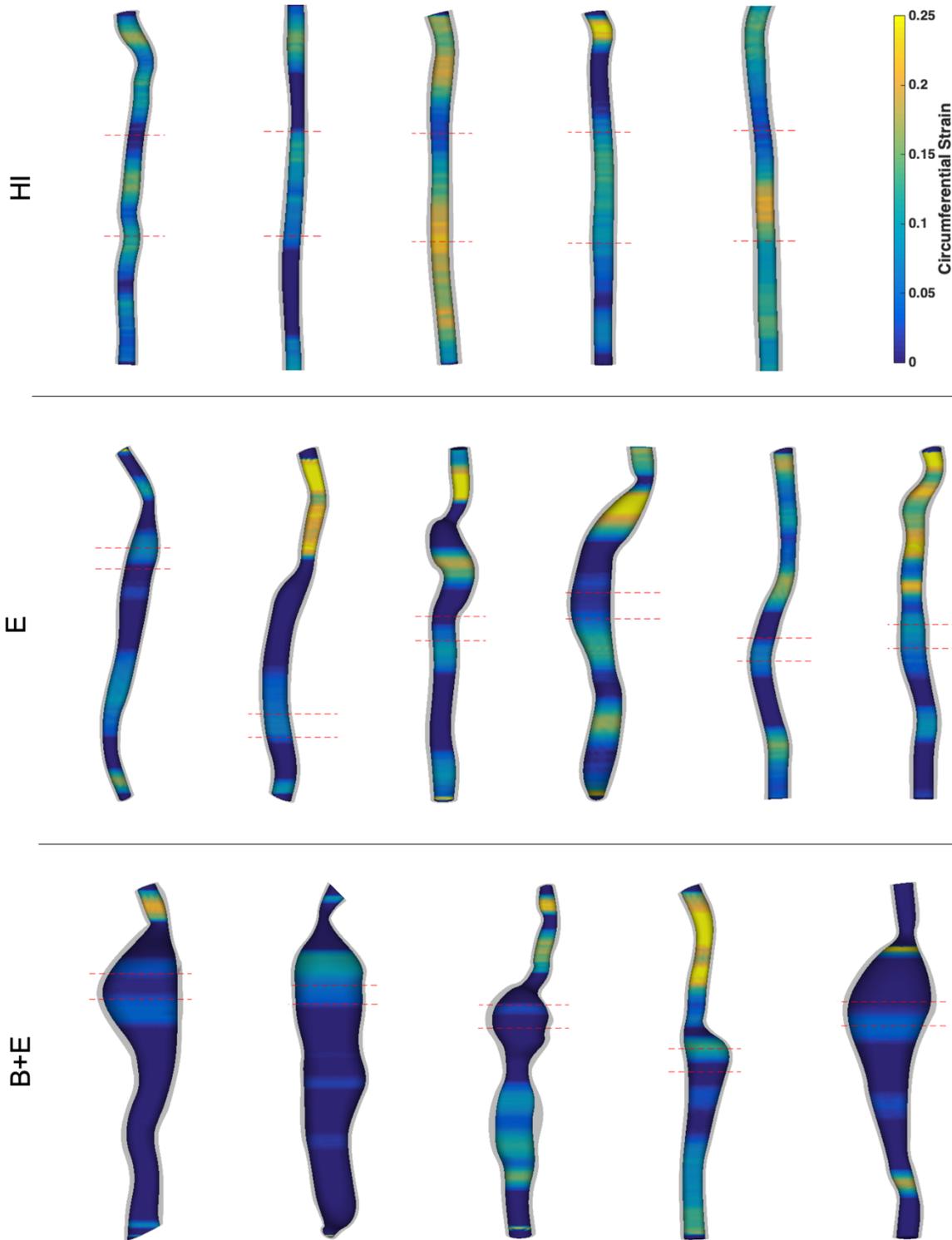
Figure S2. Day 28 Strain Maps for all animals. Dashed red lines indicate area averaged for numerical comparisons, 4 mm in height for HI, 1 mm in height for E and B+E. Infrarenal aorta models are oriented with proximal end toward the top of the page.
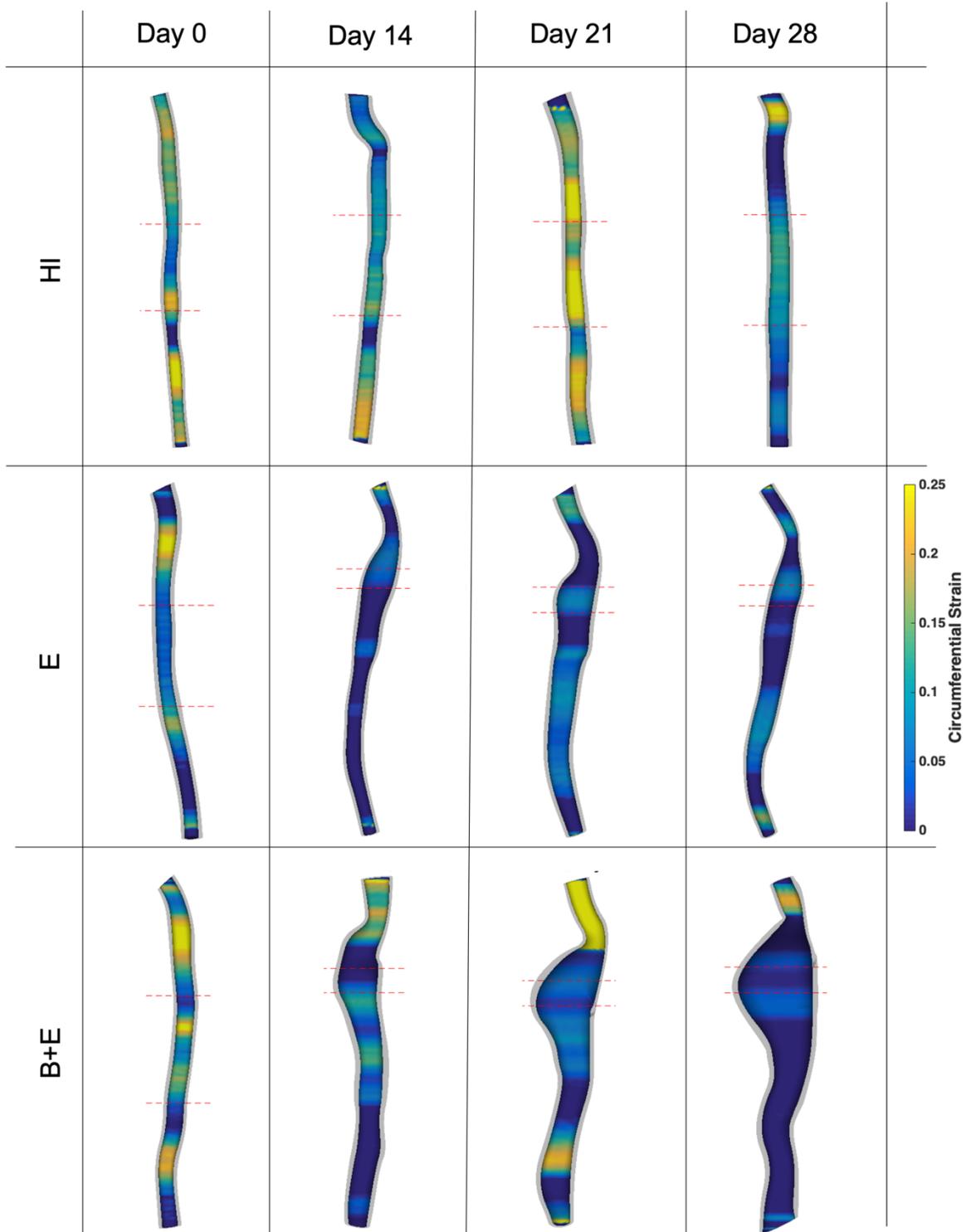
Figure S3. Strain Maps for Representative Animals Throughout the Study. Dashed red lines indicate area averaged for numerical comparisons, 4 mm in height for HI, 1 mm in height for E and B+E. Infrarenal aorta models are oriented with proximal end toward the top of the page.

REFERENCES

[1]   E. L. Chaikof *et al.*, "The Society for Vascular Surgery practice guidelines on the care of patients with an abdominal aortic aneurysm," *Journal of Vascular Surgery,* vol. 67, no. 1, pp. 2-77, Jan 2018, doi: 10.1016/j.jvs.2017.10.044.

[2]   M. J. Sweeting, S. G. Thompson, L. C. Brown, J. T. Powell, and R. Collaborators, "Meta-analysis of individual patient data to examine factors affecting growth and rupture of small abdominal aortic aneurysms," *British Journal of Surgery,* vol. 99, no. 5, pp. 655-665, May 2012, doi: 10.1002/bjs.8707.

[3]   B. Keisler and C. Carter, "Abdominal Aortic Aneurysm," *American Family Physician,* vol. 91, no. 8, pp. 538-543, Apr 2015.

[4]   D. C. Guo, C. L. Papke, R. M. He, and D. M. Milewicz, "Pathogenesis of thoracic and abdominal aortic aneurysms," *Annals of the New York Academy of Sciences,* vol. 1085, pp. 339-352, 2006, doi: 10.1196/annals.1383.013.

[5]   I. Hameed, E. M. Isselbacher, and K. A. Eagle, "Aortic Aneurysms," in *Comprehensive Cardiovascular Medicine in the Primary Care Setting*, P. Toth and C. Cannon Eds., (Contemporary Cardiology). Totowa, NJ: Humana Press, 2011, pp. 391-409.

[6]   M. Carmo *et al.*, "Alteration of elastin, collagen and their cross-links in abdominal aortic aneurysms," *European Journal of Vascular and Endovascular Surgery,* vol. 23, no. 6, pp. 543-549, Jun 2002, doi: 10.1054/ejvs.2002.1620.

[7]   P. B. Dobrin, W. H. Baker, and W. C. Gley, "Elastolytic and Collagenolytic Studies of Arteries - Implications for the Mechanical-Properties of Aneurysms," *Archives of Surgery,* vol. 119, no. 4, pp. 405-409, 1984.

[8]   I. M. Nordon, R. J. Hinchliffe, I. M. Loftus, and M. M. Thompson, "Pathophysiology and epidemiology of abdominal aortic aneurysms," *Nature Reviews Cardiology,* vol. 8, no. 2, pp. 92-102, Feb 2011, doi: 10.1038/nrcardio.2010.180.

[9]   N. Sakalihasan, A. Heyeres, B. V. Nusgens, R. Limet, and C. M. Lapiere, "Modifications of the Extracellular-Matrix of Aneurysmal Abdominal Aortas as a Function of Their Size," *European Journal of Vascular Surgery,* vol. 7, no. 6, pp. 633-637, Nov 1993, doi: 10.1016/s0950-821x(05)80708-x.

[10]   K. D. Rizas, N. Ippagunta, and M. D. Tilson, "Immune Cells and Molecular Mediators in the Pathogenesis of the Abdominal Aortic Aneurysm," *Cardiology in Review,* vol. 17, no. 5, pp. 201-210, Sep-Oct 2009, doi: 10.1097/CRD.0b013e3181b04698.

[11]   A. Maier, M. W. Gee, C. Reeps, J. Pongratz, H. H. Eckstein, and W. A. Wall, "A Comparison of Diameter, Wall Stress, and Rupture Potential Index for Abdominal Aortic Aneurysm Rupture Risk Prediction," *Annals of Biomedical Engineering,* vol. 38, no. 10, pp. 3124-3134, Oct 2010, doi: 10.1007/s10439-010-0067-6.

[12]   R. M. Greenhalgh *et al.*, "Endovascular versus Open Repair of Abdominal Aortic Aneurysm," *New England Journal of Medicine,* vol. 362, no. 20, pp. 1863-1871, May 2010, doi: 10.1056/NEJMoa0909305.

[13]   M. F. Bath, D. Sidloff, A. Saratzis, M. J. Bown, and U. K. A. G. S. investi, "Impact of abdominal aortic aneurysm screening on quality of life," *British Journal of Surgery,* vol. 105, no. 3, pp. 203-208, Feb 2018, doi: 10.1002/bjs.10721.

[14]   P. M. Brown, D. T. Zelt, and B. Sobolev, "The risk of rupture in untreated aneurysms: The impact of size, gender, and expansion rate," *Journal of Vascular Surgery,* vol. 37, no. 2, pp. 280-283, Feb 2003, doi: 10.1067/mva.2003.119.

[15]   S. Anidjar, J. L. Salzmann, D. Gentric, P. Lagneau, J. P. Camilleri, and J. B. Michel, "Elastase-Induced Experimental Aneurysms in Rats," *Circulation,* vol. 82, no. 3, pp. 973-981, Sep 1990, doi: 10.1161/01.cir.82.3.973.

[16]   A. K. Ramaswamy *et al.*, "Molecular Imaging of Experimental Abdominal Aortic Aneurysms," *Scientific World Journal,* 2013, Art no. 973150, doi: 10.1155/2013/973150.

[17]   A. C. Chiou, B. Chiu, and W. H. Pearce, "Murine aortic aneurysm produced by periarterial application of calcium chloride," *Journal of Surgical Research,* vol. 99, no. 2, pp. 371-376, Aug 2001, doi: 10.1006/jsre.2001.6207.

[18]   A. Daugherty, M. W. Manning, and L. A. Cassis, "Angiotensin II promotes atherosclerotic lesions and aneurysms in apolipoprotein E-deficient mice," *Journal of Clinical Investigation,* vol. 105, no. 11, pp. 1605-1612, Jun 2000, doi: 10.1172/jci7818.

[19]   G. Lu *et al.*, "A novel chronic advanced stage abdominal aortic aneurysm murine model," *Journal of Vascular Surgery,* vol. 66, no. 1, pp. 232-242.e4, 2017, doi: 10.1016/j.jvs.2016.07.105.

[20]   A. B. M. Wilmink, M. Forshaw, C. R. G. Quick, C. S. Hubbard, and N. E. Day, "Accuracy of serial screening for abdominal aortic aneurysms by ultrasound," *Journal of Medical Screening,* vol. 9, no. 3, pp. 125-127, 2002, doi: 10.1136/jms.9.3.125.

[21]   A. H. Soepriatna, F. W. Damen, P. P. Vlachos, and C. J. Goergen, "Cardiac and respiratory-gated volumetric murine ultrasound," *International Journal of Cardiovascular Imaging,* vol. 34, no. 5, pp. 713-724, May 2018, doi: 10.1007/s10554-017-1283-z.

[22]   F. W. Damen *et al.*, "High-Frequency 4-Dimensional Ultrasound (4DUS): A Reliable Method for Assessing Murine Cardiac Function," *Tomography,* vol. 3, no. 4, pp. 180-187, Dec 2017, doi: 10.18383/j.tom.2017.00016.

[23]   H. L. Cebull, A. H. Soepriatna, J. J. Boyle, S. M. Rothenberger, and C. J. Goergen, "Strain mapping from 4D ultrasound reveals complex remodeling in dissecting murine abdominal aortic aneurysms," *Journal of Biomechanical Engineering,* Mar 6 2019, doi: 10.1115/1.4043075.

[24]   S. Pappu, A. Dardik, H. Tagare, and R. J. Gusberg, "Beyond fusiform and saccular: A novel quantitative tortuosity index may help classify aneurysm shape and predict aneurysm rupture potential," *Annals of Vascular Surgery,* vol. 22, no. 1, pp. 88-97, Jan 2008, doi: 10.1016/j.avsg.2007.09.004.

[25]   H. Zhang, V. O. Kheyfets, and E. A. Finol, "Robust infrarenal aortic aneurysm lumen centerline detection for rupture status classification," *Medical Engineering & Physics,* vol. 35, no. 9, pp. 1358-1367, Sep 2013, doi: 10.1016/j.medengphy.2013.03.005.

[26]   S. A. Parikh *et al.*, "Decision Tree Based Classification of Abdominal Aortic Aneurysms Using Geometry Quantification Measures," *Annals of Biomedical Engineering,* vol. 46, no. 12, pp. 2135-2147, Dec 2018, doi: 10.1007/s10439-018-02116-w.

[27]   W. M. Lai, D. Rubin, and E. Krempl, "CHAPTER 3 - Kinematics of a Continuum," in *Introduction to Continuum Mechanics (Fourth Edition)*. Boston: Butterworth-Heinemann, 2010, pp. 69-153.

[28]   T. J. Chung, *General Continuum Mechanics*, 2nd ed. New York: Cambridge University Press, 2007.

[29]   J. N. Reddy, *An Introduction to Continuum Mechanics*, 2nd ed. New York: Cambridge University Press, 2013.

[30]   C. J. Goergen, B. L. Johnson, J. M. Greve, C. A. Taylor, and C. K. Zarins, "Increased anterior abdominal aortic wall motion: Possible role in aneurysm pathogenesis and design of endovascular devices," *Journal of Endovascular Therapy,* vol. 14, no. 4, pp. 574-584, Aug 2007, doi: 10.1177/152660280701400421.

[31]   P. Bihari *et al.*, "Strain Measurement of Abdominal Aortic Aneurysm with Real-time 3D Ultrasound Speckle Tracking," *European Journal of Vascular and Endovascular Surgery,* vol. 45, no. 4, pp. 315-323, Apr 2013, doi: 10.1016/j.ejvs.2013.01.004.

[32]   K. Karatolios *et al.*, "Method for Aortic Wall Strain Measurement With Three-Dimensional Ultrasound Speckle Tracking and Fitted Finite Element Analysis," *Annals of Thoracic Surgery,* vol. 96, no. 5, pp. 1664-1671, Nov 2013, doi: 10.1016/j.athoracsur.2013.06.037.

[33]   J. J. Boyle *et al.*, "Regularization-Free Strain Mapping in Three Dimensions, With Application to Cardiac Ultrasound," *Journal of Biomechanical Engineering.,* vol. 141, no. 1, p. 011010, 2019, doi: 10.1115/1.4041576.

[34]   P. E. Castle, U. M. Scheven, A. C. Crouch, A. A. Cao, C. J. Goergen, and J. M. Greve, "Anatomical location, sex, and age influence murine arterial circumferential cyclic strain before and during dobutamine infusion," *Journal of Magnetic Resonance Imaging,* vol. 49, no. 1, pp. 69-80, Jan 2019, doi: 10.1002/jmri.26232.

[35]   Y. C. Fung, "What are the residual-stresses doing in our blood-vessels?," *Annals of Biomedical Engineering,* vol. 19, no. 3, pp. 237-249, 1991, doi: 10.1007/bf02584301.

[36]   J. D. Humphrey and G. A. Holzapfel, "Mechanics, mechanobiology, and modeling of human abdominal aorta and aneurysms," *Journal of Biomechanics,* vol. 45, no. 5, pp. 805-814, Mar 2012, doi: 10.1016/j.jbiomech.2011.11.021.

[37]   Z. Li and C. Kleinstreuer, "A new wall stress equation for aneurysm-rupture prediction," *Annals of Biomedical Engineering,* vol. 33, no. 2, pp. 209-213, Feb 2005, doi: 10.1007/s10439-005-8979-2.

[38]   A. J. Hall, E. F. G. Busse, D. J. McCarville, and J. J. Burgess, "Aortic wall tension as a predictive factor for abdominal aortic aneurysm rupture: Improving the selection of patients for abdominal aortic aneurysm repair," *Annals of Vascular Surgery,* vol. 14, no. 2, pp. 152-157, Mar 2000, doi: 10.1007/s100169910027.

[39]   H. Astrand, T. Sandgren, A. R. Ahlgren, and T. Lanne, "Noninvasive ultrasound measurements of aortic intima-media thickness: Implications for in vivo study of aortic wall stress," *Journal of Vascular Surgery,* vol. 37, no. 6, pp. 1270-1276, Jun 2003, doi: 10.1016/s0741-5214(02)75344-5.

[40]   D. Farotto, P. Segers, B. Meuris, J. V. Sloten, and N. Famaey, "The role of biomechanics in aortic aneurysm management: requirements, open problems and future prospects," *Journal of the Mechanical Behavior of Biomedical Materials,* vol. 77, pp. 295-307, Jan 2018, doi: 10.1016/j.jmbbm.2017.08.019.

[41]   N. Kontopodis, K. Tzirakis, and C. V. Ioannou, "The Obsolete Maximum Diameter Criterion, the Evident Role of Biomechanical (Pressure) Indices, the New Role of Hemodynamic (Flow) Indices, and the Multi-Modal Approach to the Rupture Risk Assessment of Abdominal Aortic Aneurysms," *Annals of Vascular Diseases,* vol. 11, no. 1, pp. 78-83, 2018, doi: 10.3400/avd.ra.17-00115.

[42] M. M. Stringfellow, P. F. Lawrence, and R. G. Stringfellow, "The Influence of Aorta Aneurysm Geometry Upon Stress in the Aneurysm Wall," *Journal of Surgical Research,* vol. 42, no. 4, pp. 425-433, Apr 1987, doi: 10.1016/0022-4804(87)90178-8.

[43] S. Polzer *et al.*, "Importance of material model in wall stress prediction in abdominal aortic aneurysms," *Medical Engineering & Physics,* vol. 35, no. 9, pp. 1282-1289, Sep 2013, doi: 10.1016/j.medengphy.2013.01.008.

[44] M. F. Fillinger, S. P. Marra, M. L. Raghavan, and F. E. Kennedy, "Prediction of rupture risk in abdominal aortic aneurysm during observation: Wall stress versus diameter," *Journal of Vascular Surgery,* vol. 37, no. 4, pp. 724-732, Apr 2003, doi: 10.1067/mva.2003.213.

[45] Z. Y. Li *et al.*, "Association Between Aneurysm Shoulder Stress and Abdominal Aortic Aneurysm Expansion A Longitudinal Follow-Up Study," *Circulation,* vol. 122, no. 18, pp. 1815-1822, Nov 2010, doi: 10.1161/circulationaha.110.939819.

[46] G. Martufi *et al.*, "Local Diameter, Wall Stress, and Thrombus Thickness Influence the Local Growth of Abdominal Aortic Aneurysms," *Journal of Endovascular Therapy,* vol. 23, no. 6, pp. 957-966, Dec 2016, doi: 10.1177/1526602816657086.

[47] F. Tanios *et al.*, "Interaction of Biomechanics with Extracellular Matrix Components in Abdominal Aortic Aneurysm Wall," *European Journal of Vascular and Endovascular Surgery,* vol. 50, no. 2, pp. 167-174, Aug 2015, doi: 10.1016/j.ejvs.2015.03.021.

[48] S. S. Raut, S. Chandra, J. Shum, and E. A. Finol, "The Role of Geometric and Biomechanical Factors in Abdominal Aortic Aneurysm Rupture Risk Assessment," *Annals of Biomedical Engineering,* vol. 41, no. 7, pp. 1459-1477, Jul 2013, doi: 10.1007/s10439-013-0786-6.

[49] A. Laser *et al.*, "Differential gender- and species-specific formation of aneurysms using a novel method of inducing abdominal aortic aneurysms," *Journal of Surgical Research,* vol. 178, no. 2, pp. 1038-1045, Dec 2012, doi: 10.1016/j.jss.2012.04.073.

[50] L. I. Smith-Mungo and H. M. Kagan, "Lysyl oxidase: Properties, regulation and multiple functions in biology," *Matrix Biology,* vol. 16, no. 7, pp. 387-398, Feb 1998, doi: 10.1016/s0945-053x(98)90012-9.

[51] A. A. Yrineo *et al.*, "Murine ultrasound-guided transabdominal para-aortic injections of self-assembling type I collagen oligomers," *Journal of Controlled Release,* vol. 249, pp. 53-62, Mar 2017, doi: 10.1016/j.jconrel.2016.12.045.

[52] Y. Wang, S. E. Thatcher, and L. A. Cassis, "Measuring Blood Pressure Using a Noninvasive Tail Cuff Method in Mice," *Renin-Angiotensin-Aldosterone System: Methods and Protocols,* vol. 1614, pp. 69-73, 2017, doi: 10.1007/978-1-4939-7030-8_6.

[53] A. Updegrove, N. M. Wilson, J. Merkow, H. Z. Lan, A. L. Marsden, and S. C. Shadden, "SimVascular: An Open Source Pipeline for Cardiovascular Simulation," *Annals of Biomedical Engineering,* vol. 45, no. 3, pp. 525-541, Mar 2017, doi: 10.1007/s10439-016-1762-8.

[54] E. H. Phillips, A. A. Yrineo, H. D. Schroeder, K. E. Wilson, J. X. Cheng, and C. J. Goergen, "Morphological and Biomechanical Differences in the Elastase and AngII apoE(-/-) Rodent Models of Abdominal Aortic Aneurysms," *Biomed Research International,* 2015, Art no. 413189, doi: 10.1155/2015/413189.

[55] C. J. Goergen *et al.*, "Influences of aortic motion and curvature on vessel expansion in murine experimental aneurysms," *Arteriosclerosis, Thrombosis, And Vascular Biology,* vol. 31, no. 2, p. 270, 2011, doi: 10.1161/ATVBAHA.110.216481.

[56] J. P. V. Geest, M. S. Sacks, and D. A. Vorp, "The effects of aneurysm on the biaxial mechanical behavior of human abdominal aorta," *Journal of Biomechanics,* vol. 39, no. 7, pp. 1324-1334, 2006, doi: 10.1016/j.jbiomech.2005.03.003.

[57] M. A. F. Gsell *et al.*, "Assessment of wall stresses and mechanical heart power in the left ventricle: Finite element modeling versus Laplace analysis," *International Journal for Numerical Methods in Biomedical Engineering,* vol. 34, no. 12, Dec 2018, Art no. e3147, doi: 10.1002/cnm.3147.

[58] M. J. Feng, S. Whitesall, Y. Y. Zhang, M. Beibel, L. D'Alecy, and K. DiPetrillo, "Validation of Volume-Pressure Recording Tail-Cuff Blood Pressure Measurements," *American Journal of Hypertension,* vol. 21, no. 12, pp. 1288-1291, Dec 2008, doi: 10.1038/ajh.2008.301.

[59] Z. Szabo *et al.*, "Aortic aneurysmal disease and cutis laxa caused by defects in the elastin gene," *Journal of Medical Genetics,* vol. 43, no. 3, pp. 255-258, Mar 2006, doi: 10.1136/jmg.2005.034157.

[60] F. A. Lederle *et al.*, "Rupture rate of large abdominal aortic aneurysms in patients refusing or unfit for elective repair," *JAMA,* vol. 287, no. 22, pp. 2968-2972, Jun 2002, doi: 10.1001/jama.287.22.2968.

[61] G. Gamble, J. Zorn, G. Sanders, S. Macmahon, and N. Sharpe, "Estimation of Arterial Stiffness, Compliance, and Distensibility from M-mode Ultrasound Measurements of the Common Carotid-Artery," *Stroke,* vol. 25, no. 1, pp. 11-16, Jan 1994, doi: 10.1161/01.str.25.1.11.

[62] M. L. Liu, L. Liang, and W. Sun, "Estimation of in vivo mechanical properties of the aortic wall: A multi-resolution direct search approach," *Journal of the Mechanical Behavior of Biomedical Materials,* vol. 77, pp. 649-659, Jan 2018, doi: 10.1016/j.jmbbm.2017.10.022.

[63] E. M. J. van Disseldorp, N. J. Petterson, M. C. M. Rutten, F. N. van de Vosse, M. van Sambeek, and R. G. P. Lopata, "Patient Specific Wall Stress Analysis and Mechanical Characterization of Abdominal Aortic Aneurysms Using 4D Ultrasound," *European Journal of Vascular and Endovascular Surgery,* vol. 52, no. 5, pp. 635-642, Nov 2016, doi: 10.1016/j.ejvs.2016.07.088.

VITA

Daniel J. Romary completed his undergraduate studies at Purdue University in West Lafayette, graduating with a bachelor's degree in biomedical engineering, with highest distinction, in May 2018. He conducted undergraduate research in the laboratory of Dr. Sherry Voytik-Harbin in the field of tissue engineering prior to his master's research. Since joining Dr. Craig Goergen's Cardiovascular Imaging Research Laboratory, Romary has worked on characterizing and utilizing the BAPN-elastase model of abdominal aortic aneurysms.

Throughout his time at Purdue, Romary has taken on numerous leadership positions outside of research. Most notably, he served as the Governor-appointed student trustee on Purdue's Board of Trustees from 2017 to 2019.

Romary received the Charles C. Chappelle Fellowship, was named the 2018 G.A. Ross Outstanding Senior Man, and was the recipient of the 2016 Charles Wayne Sullivan Outstanding Biomedical Engineering Sophomore award.

Following graduation, he plans to attend medical school and practice medicine in the cardiovascular field.

PUBLICATIONS

D. J. Romary, A. G. Berman, C. J. Goergen, "High Frequency Murine Ultrasound Provides Enhanced Metrics of BAPN-Induced AAA Growth," 2019 (In preparation)

A. G. Berman, **D. J. Romary**, M. Wigand, S. Patnaik, E. Finol, and C. J. Goergen, "Longitudinal Ultrasound Assessment of Murine Aneurysm Expansion and Intraluminal Thrombus Formation," 2019 (In preparation)

N. M. Patel, J. N. Ray, **D. J. Romary**, A. M. Sacopulous, "A Breastfeeding Simulation System," United States Patent Pending, 2019